Supplementary Information

1. The effect of the $\delta^{13}C(CH_4)$ seasonal cycle

CH_4 and $\delta^{13}C(CH_4)$ undergo seasonal cycles (Miller et al., 2002, Tyler et al., 2007, Dugoklencky et al., 2009), which are recorded in the upper firn. However, the inverse model cannot reconstruct the seasonal signal (see: Wang et al., 2012 for further discussion) thus it has to be assessed separately. The amplitude of the seasonal signal at the SH sites is very small and thus does not significantly affect the firn profiles from Antarctica. Therefore, the sensitivity to seasonality was only examined for the NH sites using the model in the forward mode. Model runs were performed for an atmospheric scenario with (Fig. S1: black lines) and without (Fig. S1: colored lines) seasonality and the difference between the two model results was used to correct the firn data for seasonality. These corrected values were used as input in the inverse model.

Note that near-surface $\delta^{13}C(CH_4)$ data in Devon Island firn are distinctly lower than at other sites, although seasonality has a weak impact. Diffusivity at Devon Island is smaller than at all other sites, and stronger CH_4 trends are observed in the upper firn than at other sites (Witrant et al., 2012). In relation with the melt layers, firn fractionation may already operate and be under-estimated by the model in the upper Devon Island firn.

2. Sensitivity to uncertainties on the CH_4 scenario

A reconstructed atmospheric CH_4 scenario is used as input for the model. This scenario is based on direct atmospheric measurements from continuous

atmospheric monitoring from the NOAA-ESRL network and from high-resolution firn/ice core measurement from the high accumulation site of Law Dome, Antarctica (Etheridge et al., 1998, MacFarling Meure et al., 2006). Based on these data, two CH_4 scenarios were built for the Northern (Buizert et al., 2012) and Southern (Witrant et al., 2012) hemispheres. As shown in Section 5.3 of the main paper, the temporal change in the CH_4 mixing ratio is responsible for a large fraction of the $\delta^{13}C(CH_4)$ variations in the firn.

In order to evaluate the sensitivity of $\delta^{13}C(CH_4)$ to the precise shape of the CH_4 scenario, the model was forced with the minimum and maximum values of the CH_4 scenarios. The results depicted in Fig. S2, show that the scenarios inferred by the minimum (left panels: green line) and the maximum (left panels: purple line) CH_4 trends are within the uncertainty envelopes of our $\delta^{13}C(CH_4)$ best-guess scenario. However, the uncertainty on the CH_4 scenario affects the slope of the reconstructed $\delta^{13}C(CH_4)$ trend and is a possible explanation for the difference between our results and Cape Grim air archive data.

3. Sensitivity to the regularization term

Since reconstructing atmospheric scenarios from firn air data is an under-constrained approach (less data than degrees of freedom), additional information is required to obtain a unique solution. This additional information is provided as a regularization term "k^2" which controls the smoothness of the solution (Rommelaere et al., 1997). Higher values of k^2 lead to smoother $\delta^{13}C(CH_4)$ scenarios while low values of k^2 lead to more variable solutions which fit more of the

variability of firn air data (which are also associated with an analytical error). As the timescale of $\delta^{13}C(CH_4)$ variations in the atmosphere is long (Tans, 1997), the regularization term has to be carefully chosen to yield a smooth scenario that still fits the data within the uncertainty.

The choice of the optimal values of k^2 is an important issue recently improved in Witrant and Martinerie, (2013) using a robustness-oriented statistical technique. In order to investigate the sensitivity of $\delta^{13}C(CH_4)$ to the regularization term, we vary it by several orders of magnitude. Fig. S3ac, shows the effect of increasing the regularization term by a factor 100 (long-dashed blue lines) and by a factor 10 (short-dashed blue lines) and by decreasing it by a factor 100 (long-dashed green lines) and 10 (short-dashed green line). For the SH sites, the difference among the scenarios, long-dashed line, short-dashed line and full-line (best-guess scenario) is very small. For the NH sites, the difference is larger, but the scenarios all fall within the uncertainty envelope of the optimal scenario, except for the early part of the profile for the factor 100 decrease. Fig. S3 shows that the number of different sites constraining the model is important. For the SH, where 7 qualitatively different sites are used as input for the multi-site inversion, the regularization term does not affect the $\delta^{13}C(CH_4)$ scenario significantly, whereas for the NH with only 3 sites with very similar profiles the scenario is less well constrained.

4. Deep firn data

In the multisite scenario reconstruction, the deepest data-points at each site

were excluded, because the correction for isotopic fractionation is very uncertain in the deep firn. Two different ways of excluding deep firn data were used. The first method is used in the main article: the data points showing the strongest deviations from the modeled isotopic fractionation in firn are removed (Fig. 5 of the main paper, also shown in Fig. S4, black lines). Alternatively (second method used here) all data below the lock-in depth (LIDgas in Table 2 of Witrant et al., 2012) are removed. The results are provided in Fig. S4, red and green lines. Both methods show very similar results. However, removing all data points below the LID reduces the length of the period of the reconstructed atmospheric trend (more firn data are excluded).

5. Accounting for inter-laboratory calibration differences

Inconsistencies between different datasets can arise due to calibration scale differences between laboratories. Since the largest amount of data presented here was measured at the LGGE, all the results are converted to the LGGE scale, based on the following arguments. Note that the LGGE system is no longer operational prohibiting direct intercalibration with the other systems. 10 firn gas samples from NGRIP have been measured by IMAU. Those samples were covering the same depth range as the samples measured at the LGGE 6 years earlier but were not the same set of samples. However, all measurements of firn air from similar depths have been compared and the average $\delta^{13}C(CH_4)$ difference measured between IMAU and LGGE is 0.14 ± 0.07‰. The IMAU data are corrected for this offset.

To link the data from CIC to the LGGE scale, CIC measured NEEM 2008 firn samples from the European hole (NM-EU-08), which were measured at IMAU and an average difference of 0.14+/-0.02 ‰ has been measured between the IMAU and CIC, yielding a difference of 0 +/-0.07 ‰ between CIC and LGGE. The intercalibration is supported by Sperlich et al. (2012) and (2013) who referenced the CIC setup directly to the VPDB scale, to optimize the measurement accuracy.

No systematic differences between LGGE, NIWA and CSIRO were reported for $\delta^{13}C(CH_4)$ anaylsis in previous studies (Aballain, 2002, page 82 and S. Bernard, PhD Thesis, 2004).

The differences between the different measurement systems and the LGGE are summarized in Table S1. These intercalibration offsets are of the order of the analytical precision of individual laboratories and smaller than the reconstructed temporal trends.

6. Forward model forced with the Cape Grim-DEO8 scenario

As an alternative way to assess the consistency between previously published data and the complete firn air dataset, an atmospheric scenario was built solely from atmospheric and DE08 data (Fig. S5, left panel) and used as input to the LGGE-GIPSA forward model of gas transport in firn. Note that NIWA data was preferred to NOAA data here because inter-calibration tests showed no significant discrepancies between LGGE, CSIRO and NIWA data (Aballain, 2002, page 82), whereas no direct comparison with LGGE data is available for NOAA data. A recent comparison of NIWA and NOAA atmospheric data series suggest a shift of 0.132±0.22 ‰ (Levin et al., 2012). Fig. S5

shows that a scenario using NIWA, Cape Grim and DEO8 as input in the forward model leads to large discrepancies between the data points and the modeled concentrations in firn (Fig. S5b). This shows that using DEO8, even though it is a high accumulation rate site, to build a reference $\delta^{13}CH_4$ atmospheric trend does not improve the consistency between the datasets. The DE08 firn was sampled in 1993. The two next sampling were performed at South Pole (SPO95) and Vostok (VOS) in 1995. These similar drill dates imply that upper firn air samples at those three sites have similar ages. However, simulating $\delta^{13}C(CH_4)$ at SPO95 and VOS with a DE08 based atmospheric scenario leads to large differences with the data well above the lock-in depth, where firn fractionation is limited. Thus, uncertainties associated to intercalibration offsets or associated to experimental issues (Kr interference) between the different laboratories could also cause the discrepancies observed.

7. Dispersive mixing tests

The possible occurrence of dispersive or non-fractionating transport within the lock-in zone has been recently introduced and formulated as a gas independent diffusive term (Severinghaus et al., 2010, Supplement). This term is similar to the term used to represent convective mixing in the upper firn. In the absence of a quantitative criterion to discriminate between molecular diffusion (characterised by a gas dependent diffusion coefficient D_{molec}) and dispersive transport (characterized by a gas independent diffusion coefficient D_{eddy}), different relative fractions of diffusion versus dispersion terms have been used (Buizert et al., 2012; Trudinger et al., 2013). It should be noted that the differences between our results and previous

$\delta^{13}C(CH_4)$ firn air studies cannot be caused by the effect of dispersive transport in the lock-in zone because this new concept was not used in the earlier studies (Francey et al., 1999, Bräunlich et al., 2001, Sowers, GBC, 2005).

We tested the effect of a potential dispersive transport in the LIZ by splitting the diffusivity for $^{13}CH_4$ into a dispersive fraction (where the diffusion coefficient in free air of $^{12}CH_4$ is used for both isotopologues) and the normal molecular diffusion fraction where the different diffusion coefficients in free air of $^{12}CH_4$ and $^{13}CH_4$ are used. The relative fractions of the two diffusive terms as a function of D_{total} were scaled to the NEEM-EU CIC model diffusivities in Buizert et al. (2012). For $^{12}CH_4$ the diffusivity does not change in this setup. This test is similar to Scenario 1 in Buizert et al., (2012) and does not require re-tuning diffusivity profiles at all sites. This implementation method is motivated by the fact that using the CIC model dispersive mixing fraction also for $^{12}CH_4$ would require re-tuning diffusivity profiles at all sites: a drawback of representing dispersive mixing as a gas independent diffusive term is that all gases are not affected equally. Buizert et al. (2012) have chosen CO_2 as the reference gas for which dispersive mixing and molecular diffusion have the same effect. Hence CO_2 is not affected by dispersive mixing whereas $\delta^{13}C(CO_2)$ is. In the case of CH_4, both CH_4 and $\delta^{13}C(CH_4)$ are affected.

Based on the fact that DE08 is less affected by firn fractionation than other sites (see Section 5.4 of the main article and Buizert et al., 2012), we performed the SH dispersive mixing test using the DE08 and atmospheric data based scenario described in the previous section, and the forward firn model. The comparison of Fig. S5b (no dispersive mixing) and Fig. S6b (with dispersive mixing) confirms the

weaker impact of firn fractionation in the lock-in zone at DE08 compared to other sites. However, major discrepancies between model results and firn data above the lock-in depth remain (e.g. at Vostok and South Pole 1995, as discussed in Section 5.4), thus dispersive mixing in the lock in zone does not allow to reconcile the DE08 firn and ice based scenario with results at other sites.

No high accumulation rate site based trend scenario is available for the NH, thus the NH dispersive mixing test was performed using our inverse scenario model and Kr corrected data (Fig. S7). The comparison of those results with Fig. 8 of the main article shows that the early part of the reconstructed atmospheric trend is affected by dispersive mixing. This is consistent with the calculated estimate of Buizert et al. (2012) of about 0.5 ‰ uncertainty for $\delta^{13}C(CH_4)$ in the lock-in zone.

SUPPLEMENTARY REFERENCES

Bräunlich, M., Aballain, O., Marik, T., Jockel, P., Brenninkmeijer, C. A. M., Chappellaz, J., Barnola, J. M., Mulvaney, R., and Sturges, W. T.: Changes in the global atmospheric CH_4 budget over the last decades inferred from $\delta^{13}C$ and δD isotopic analysis of Antarctic firn air, J. Geophys. Res., 106, 20465-20481, DOI:10.1029/2001JD900190, 2001.

Buizert, C. et al.: Gas transport in firn: multiple-tracer characterisation and model intercomparison for NEEM, Northern Greenland, Atmos. Chem. Phys., 12, 4259-4277, DOI:10.5194/acp-12-4259-2012, 2012.

Dlugokencky, E. J., Bruhwiler, L., White, J. W. C., Emmons, L. K., Novelli, P. C., Montzka, S. A., Masarie, K. A., Lang, P. M., Crotwell, A. M., Miller, J. B., and Gatti, L. V.: Observational constraints on recent increases in the atmospheric CH_4 burden, Geophys. Res. Lett., 36, L18803, DOI:18810.11029/12009gl039780, 2009.

Etheridge, D. M., Steele, L. P., Francey, R. J., and Langenfelds, R. L.: Atmospheric CH_4 between 1000 AD and present: Evidence of antropogenic emissions and climatic variability, J. Geophys. Res., 103, 15979-15993, 1998.

Ferretti, D., Miller, J., White, J., Etheridge, D., Lassey, K., Lowe, D., Allan, B., MacFarling, C., Dreier, M., Trudinger, C., and Ommen, T. v.: Unexpected changes to

the global CH_4 budget over the past 2000 years, Science, 309, 864-867, DOI: 10.1126/science.1115193, 2005.

Francey, R., Manning, M.R., Allison, C.E., Coram, S.A., Etheridge, D.M., Langenfelds, Lowe, D.C., and Steele, L.P.: A history of $\delta^{13}C$ in atmospheric CH_4 from the Cape Grim Air Archive and Antarctic firn air. J. Geophys. Res., 104, 631-643, 1999.

Levin, I., Veidt, C., Vaughn, B. H., Brailsford, G., Bromley, T., Heinz, R., Lowe, D., Miller, J. B., Poss, C., and White, J. W. C.: No inter-hemispheric $\delta^{13}C(CH_4)$ trend observed, Nature, 486, E3-E4, 2012.

Lowe, D.C., Brenninkmeijer, A.M., Tyler, S.C., Dlugokencky, E.J.: Determination of the Isotopic Composition of Atmospheric Methane and its application in the Antarctic, J. Geophys. Res., 96, 15455-15467, 1991.

MacFarling Meure, C., Etheridge, D., Trudinger, C., Steele, P., Langenfelds, R., Ommen, T. v., Smith, A., and Elkins, J.: Law Dome CO_2, CH_4 and N_2O ice core records extended to 2000 years BP Geophys. Res. Lett., 33, L14810, DOI:14810.11029/12006GL026152, 2006.

Miller, J. B., Mack, K. A., Dissly, R., White, J. W. C., Dlugokencky, E. J., and Tans, P. P.: Development of analytical methods and measurements of $\delta^{13}C$ in atmospheric CH_4 from the NOAA/CMDL global air sampling network, J. Geophys. Res., 107, 4178, DOI: 10.1029/2001JD000630, 2002.

Rommelaere, V., Arnaud, L., and Barnola, J.-M.: Reconstructing recent atmospheric trace gas concentrations from polar firn and bubbly ice data by inverse methods, J. Geophys. Res., 102, 30 069–30 083, 1997.

Severinghaus, J. P., Albert, M. R., Courville, Z. R., Fahnestock, M. A., Kawamura, K., Montzka, S. A., Muehle, J., Scambos, T. A., Shields, E., Shuman, C. A., Suwa, M., Tans, P. and Weiss, R. F.: Deep air convection in the firn at a zero-accumulation site, Central Antarctica, Earth Planet. Sci. Lett., 293, 359–367, doi:10.1016/j.epsl.2010.03.003, 2010.

Sowers, T., Bernard, S., Aballain, O., Chappellaz, J., Barnola, J. M., and Marik, T.: Records of the $\delta^{13}C$ of atmospheric CH_4 over the last 2 centuries as recorded in Antarctic snow and ice, Global Biogeochem. Cycles. 19, 493–503, DOI:2010.1029/2004GB002408, 2005.

Sperlich, P., Guillevic, M., Buizert, C., Jenk, T. M., Sapart, C. J., Schaefer, H., Popp, T. J., and Blunier, T.: A combustion setup to precisely reference $\delta^{13}C$ and $\delta^{2}H$ isotope ratios of pure CH_4 to produce isotope reference gases of $\delta^{13}C$-CH_4 in synthetic air, Atmos. Meas. Tech., 5, 2227-2236, 2012.

Sperlich, P., Buizert, C., Jenk, T. M., Sapart, C. J., Prokopiou, M., Röckmann, T., and Blunier, T.: An automated setup to measure paleoatmospheric $\delta^{13}C$-CH_4, $\delta^{15}N$-N_2O and $\delta^{18}O$-N_2O in one ice core sample, Atmos. Meas. Tech. Discuss., 6, 2183-2225, 2013.

Tans, P. P.: A note on isotopic ratios and the global atmospheric methane budget, Gl. Biogeochem. Cycles, 11, 77-81, 1997.

Trudinger, C. M., Enting, I. G., Rayner, P. J., Etheridge, D. M., Buizert, C., Rubino, M., Krummel, P. B., and Blunier, T.: How well do different tracers constrain the firn diffusivity profile?, Atmos. Chem. Phys., 13, 1485-1510, 2013

Tyler, S. C., Rice, A. L., and Ajie, H. O.: Stable isotope ratios in atmospheric CH_4: Implications for seasonal sources and sinks, J. Geophys. Res., 112, D03303, DOI:10.1029/2006JD007231, 2007.

Wang, Z., Chappellaz, J., Martinerie, P., Park, K., Petrenko, V., Witrant, E., Emmons, L. K., Blunier, T., Brenninkmeijer, C. A. M., and Mak, J. E.: The isotopic record of Northern Hemisphere atmospheric carbon monoxide since 1950: implications for the CO budget, Atmos. Chem. Phys., 12, 4365-4377, doi:10.5194/acp-12-4365-2012, 2012.

Witrant, E., Martinerie, P., Hogan, C., Laube, J. C., Kawamura, K., Capron, E., Montzka, S. A., Dlugokencky, E. J., Etheridge, D., Blunier, T., and Sturges, W. T.: A new multi-gas constrained model of trace gas non-homogeneous transport in firn: evaluation and behavior at eleven polar sites, Atmos. Chem. Phys., 12, 11465-11483, doi:10.5194/acp-12-11465-2012, 2012.

Witrant, E. and Martinerie, P., "Input Estimation from Sparse Measurements in LPV Systems and Isotopic Ratios in Polar Firns",Proc. of the IFAC Joint Symposium on SSSC, TDS and FDA, Grenoble, France, Feb. 4-6, 2013.

Table S1: Intercalibration difference in $\delta^{13}C(CH_4)$ between LGGE and other laboratories.

Laboratories	IMAU	CIC	CSIRO	NIWA	NOAA
LGGE	0.14 +/-0.07 ‰	0 +/- 0.07 ‰	No systematic difference	No systematic difference	No intercalibration available

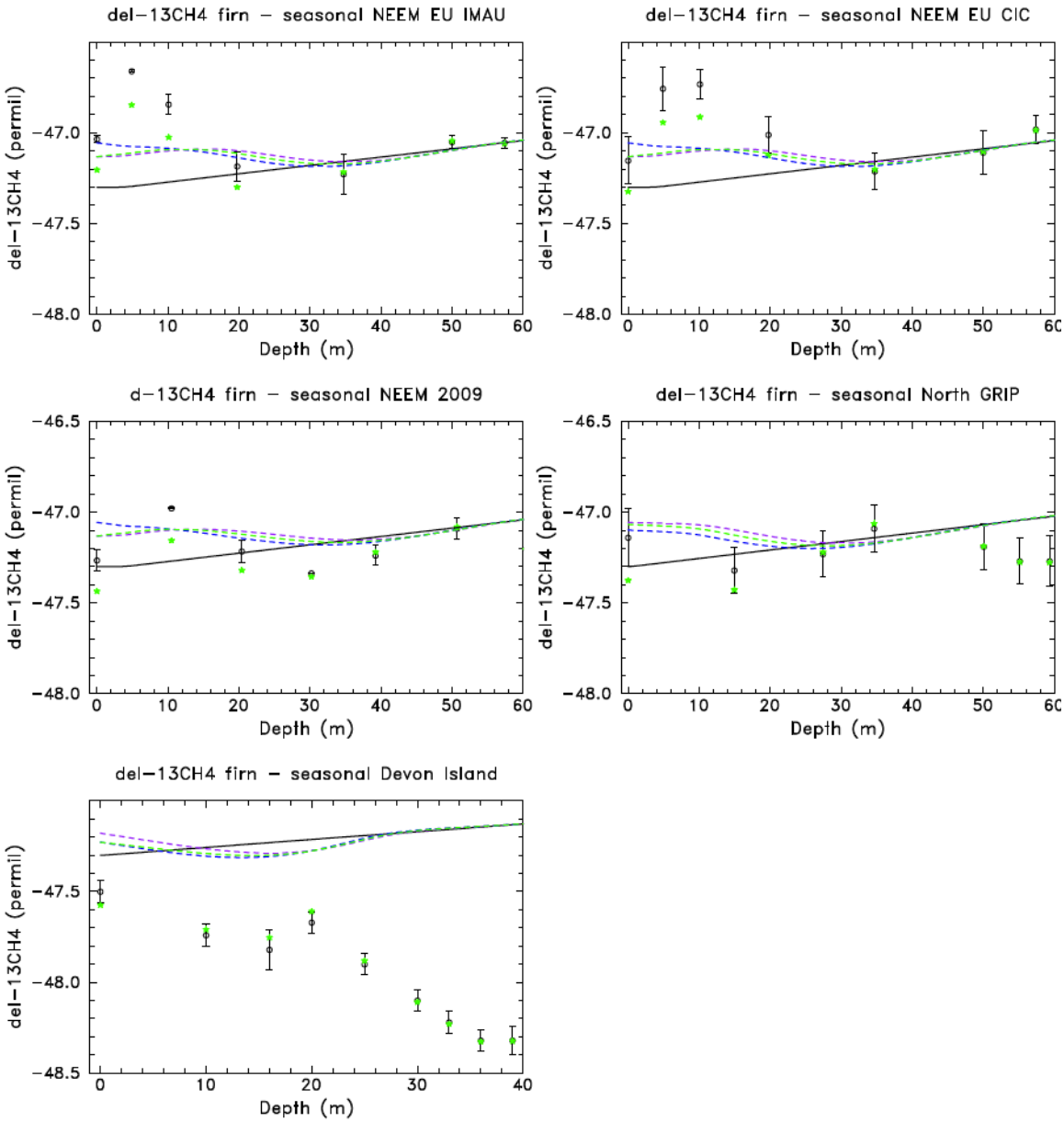

Figure S1: Model estimate of the effect of seasonality on $\delta^{13}C(CH_4)$ in firn. Measured isotopic ratios are shown as black circles with error bars. Simulated values with constant atmospheric trends in $\delta^{13}C(CH_4)$ and without seasonal cycle are plotted as black lines, simulated values with constant atmospheric trends and perpetual mean seasonal cycle are plotted as green dashed lines. The increasing isotopic ratios with depth obtained from constant scenarios (black lines) illustrate the effect of gravitational fractionation. The purple and blue dashed lines illustrate the effect of shifting the final date of the simulation (drill date) by plus or minus 15 days respectively. The green dots are the measurement values corrected for the difference between model results without seasonality (black solid lines) and with seasonality (green dashed lines).

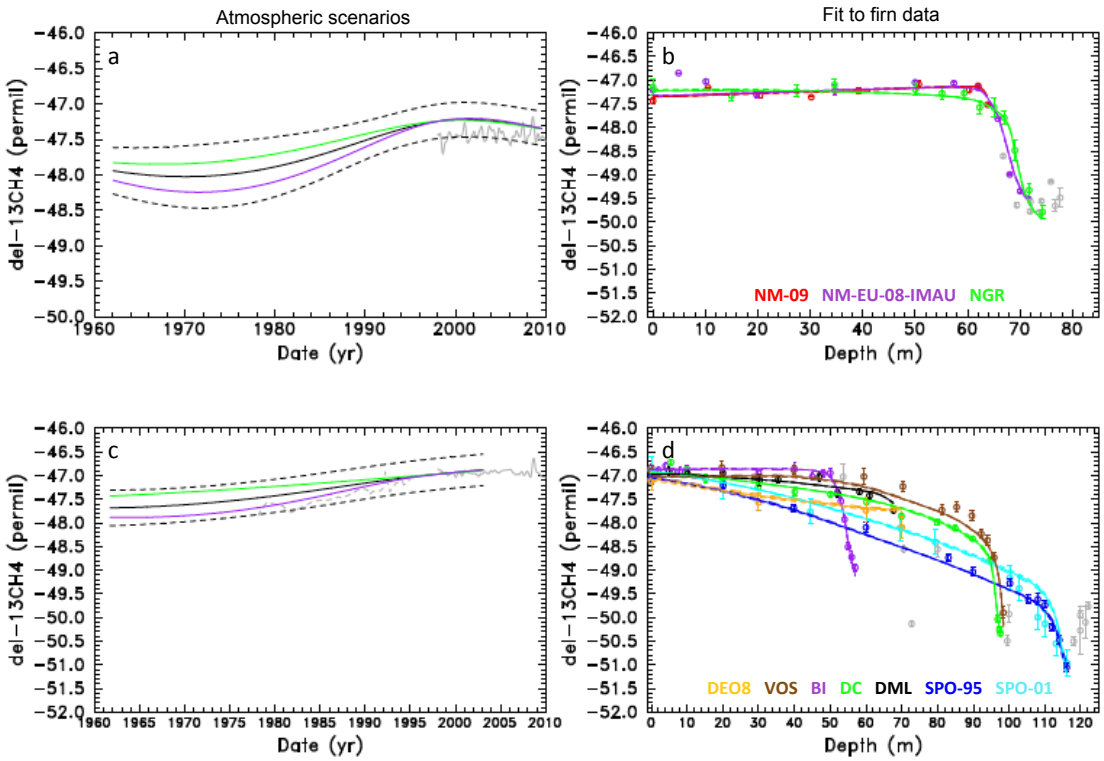

Figure S2: Multi-site $\delta^{13}C(CH_4)$ trend reconstructions (a,c) and their match to the firn data (b,d) in the NH (a,b) and SH (c,d) for different input scenarios of the historic CH_4 evolution (see text). a,c,Inferred isotope scenario for minimum (green), maximum (purple) or best estimate (black) CH_4 scenario used in the inversion. Uncertainty limits for the best estimate are shown as dashed lines. Right panels: Isotope profiles at NM-EU-08 (purple), NM-09 (red), NGR (green) and DI (black) for the NH and DE08 (orange), BI(purple), SPO-95 (dark blue), SPO-01 (light blue), DML (black), DC (green), VOS (brown) for the SH. Equal weight is given to all sites and for SPO-01 the diffusivity from SPO-95 is used. Points from the deep firn that were left out for the multi-site reconstruction are shown in grey.

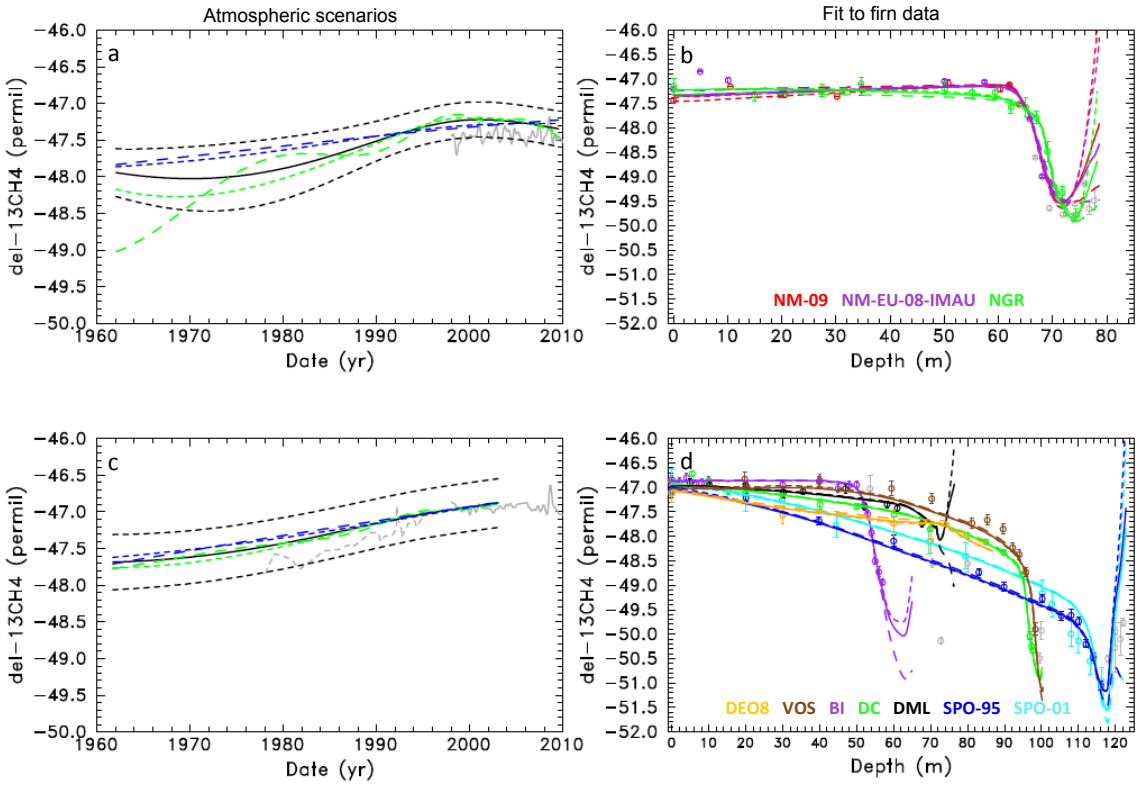

Figure S3: Sensitivity of $\delta^{13}C(CH_4)$ reconstructions to the regularization term. Multi-site $\delta^{13}C(CH_4)$ trend reconstructions (left panels) and their match of the firn data (right panels). a and c: Black lines (with dashed lines as confidence intervals) show the result with optimized regularization term k^2, which is compared to: regularization term increased by a factor of 100 (long-dashed blue line), regularization term increased by a factor of 10 (short-dashed blue line), regularization term reduced by a factor of 100 (long-dashed green line) and regularization term reduced by a factor of 10 (short-dashed green line). b and d: Comparison of model results to the data. Solid lines show the model results with the optimized regularization term, short-dashed lines the results with regularization term reduced by a factor of 100 and long-dashed lines the results with regularization term increased by a factor of 100. Equal weight for all sites and modified diffusivity for SPO-01 (using diffusivity from SPO-95) were used. Points from the deep firn that were left out for the multi-site reconstruction are shown in grey.

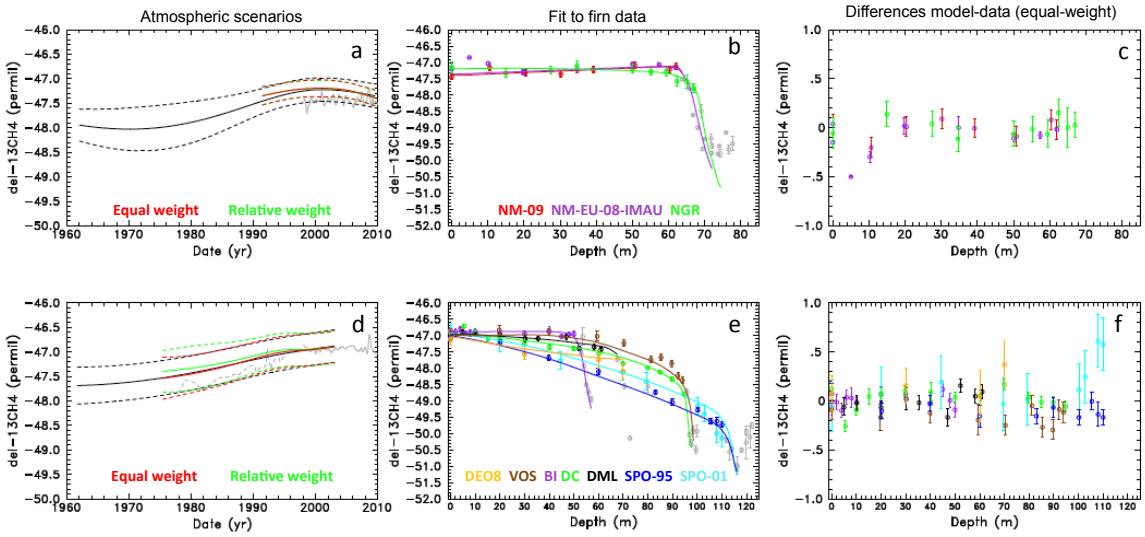

Figure S4: Multi-site $\delta^{13}C(CH_4)$ trend reconstructions (a and d), the fit to the firn data (b and e) and the difference between model-data (c and f). NH sites (a, b and c) and SH sites (d, e and f) when all data points below the LID are excluded in the inversion. Multi-site inversion with equal-weight for each site (red lines) and with single site RMS difference based weight for each site (green lines) (a,d). Optimal scenarios are shown as continuous lines and uncertainty envelopes as dashed lines. The grey curve (a,d) represents air-archive from Cape Grim (Francey et al., 1998) and continuous atmospheric monitoring data from the NOAA-ESRL network. The black lines on panels a and b represent the red lines in Fig. 5 of the main paper. When all points below the lock-in depth are excluded ,the scenarios are much shorter (red and green lines).

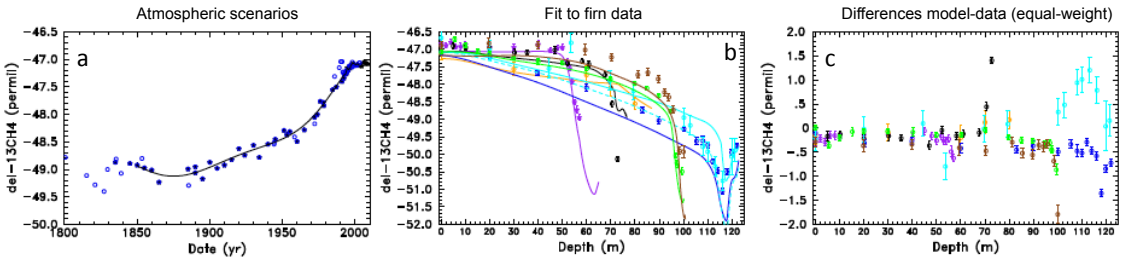

Figure S5: SH (a) atmospheric scenario for $\delta^{13}C$ (black line) based on NIWA atmospheric data at Arrival Heights (Antarctica, Lowe et al., 1991), the Cape Grim air archive (Francey et al., 1999), and DE08 firn and ice data (Ferretti et al., 2005). Black stars show the dataset used to build the scenario, blue circles show the whole Ferretti et al. (2005) dataset also including the lower accumulation rate DSS site. (b) Comparison of the firn data with model results obtained by using the panel (a) scenario as input to the LGGE-GIPSA forward model of gas transport in firn. The light blue dashed line shows results for South Pole 2001 obtained with the South Pole 1995 diffusivity. (c) model-data differences (for SP2001 with the original diffusivity). The site names and color codes are as given in the legend of Fig. 1.

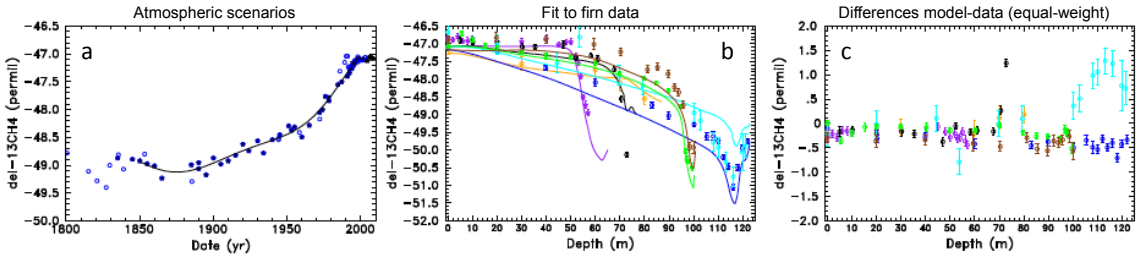

Figure S6: Dispersive mixing test for the SH sites. SH (a) atmospheric scenario for $\delta^{13}C$ (black line) based on NIWA atmospheric data at Arrival Heights (Antarctica, Lowe et al., 1991), the Cape Grim air archive (Francey et al., 1999), and DE08 firn and ice data (Ferretti et al., 2005). Black stars show the dataset used to build the scenario, blue circles show the whole Ferretti et al. (2005) dataset also including the lower accumulation rate DSS site. (b) Comparison of the firn data with model results obtained by using the panel (a) scenario as input to the LGGE-GIPSA forward model of gas transport in firn including dispersive mixing. (c) model-data differences with dispersive mixing. The site names and color codes are as given in the legend of Fig. 1.

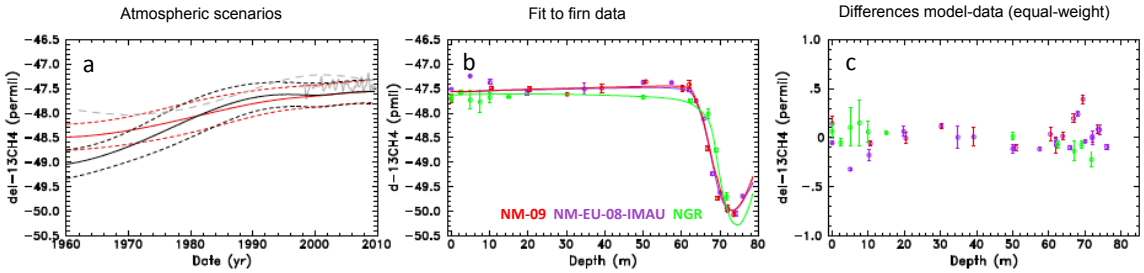

Figure S7: Dispersive mixing test for the NH sites. (a) NH multi-site $\delta^{13}C(CH_4)$ trend scenarios based on Kr corrected firn data without dispersive mixing (red curves, same as Fig. 8 of the main article) and with dispersive mixing (black curves). (b) The fit to the firn data with dispersive mixing. (c) model-data differences with dispersive mixing. The continuous grey curve (a) represents continuous atmospheric monitoring data from the NOAA-ESRL network. The dashed grey curve shows the preferred multi-site scenario based on non Kr-corrected data (red continuous line in Fig. 5a of main article).